Proc. Indian Acad. Sci. (Chem. Sci.), Vol. 97, Nos 3 & 4, October 1986, pp. 417–430.

Cyclic voltammetric studies of dioxygen-bridged dinuclear cobalt(III) complexes[§]

S ILANGOVAN and P NATARAJAN*

Department of Inorganic Chemistry, School of Chemistry, University of Madras, Guindy Campus, Madras 600 025, India

Abstract. Cyclic voltammetric studies were carried out for dioxygen-bridged dinuclear cobalt(III) complexes using platinum electrodes at different values of pH and ionic strength. Reversible electrode reactions occur particularly for the dioxygen complexes $[(phen)_2Co(\mu\text{-}O_2,NH_2)Co(phen)_2]$ $(ClO_4)_4 2H_2O$ and $[(bpy)_2Co(\mu\text{-}O_2,NH_2)Co(bpy)_2]$ $(ClO_4)_4 \cdot H_2O$ with 1,10-phenanthroline (phen) and 2,2-bipyridine (bpy) as the non-bridging ligands. For complexes with ammonia (NH_3) ethylenediamine (en) as the terminal ligands, there is quasi-reversible electrode behaviour at pH <3 due to protonation of the peroxo complexes which subsequently undergo equilibration with isomeric forms. Such behaviour is well-marked for the peroxo complex $[(en)_2Co(\mu\text{-}O_2 NH_2)Co(en)_2](NO_3)_3$. The decaammine complex $[(NH_3)_5Co(\mu\text{-}O_2)Co(NH_3)_5](NO_3)_5$ shows only a cathodic peak due to intramolecular charge transfer decomposition in solution after reduction at the electrode. Diffusion coefficients for all the dioxygen complexes were determined from the plots of I_p vs. $\nu^{1/2}$.

Keywords. Cyclic voltammetric studies; dioxygen-bridged dinuclear Co(III) complexes; superoxo complexes; peroxo complexes; coordinated dioxygen systems.

1. Introduction

Redox behaviour of dioxygen molecule in aqueous solution at different values of pH has been studied in great detail (Sawyer and Valentine 1981). It is of immense interest to study the electrodic behaviour of coordinated dioxygen systems for understanding the mechanisms of oxygenation and related biological redox reactions (McLendon and Martell 1976; Jones *et al* 1979). Considerable attention has been paid recently to these dioxygen coordinated metal complexes, since vital biological functions such as oxygen transport and many enzymatic reactions take place involving oxygen in different oxidation states (Wilkins 1971; Hayaishi 1975). Although the existence of cobalt complexes coordinated to dioxygen has been known for a long time, no specific biological functions are attributed to these species (Sykes and Weil 1970; Lever and Gray 1978). Depending upon the ligands and the conditions of oxygenation, the cobalt(II) ion forms 1 : 1 or 1 : 2 oxygen metal complexes (Basolo *et al* 1975; Jones *et al* 1979). Complexes of these types have been isolated and characterized with reference to structure, spectra and reactivity (Sykes and Weil 1970; McLendon and Martell 1976; Lever and Gray 1978; Jones *et al* 1979). Structural investigation and ESR studies of these dioxygen complexes show that the dioxygen moiety in these complexes exists in two forms namely peroxo (diamagnetic) and superoxo (paramagnetic) forms, the unpaired

[§] Dedicated to Prof. K S G Doss on his eightieth birthday.

* To whom all correspondence should be addressed.

electron mainly resides in the superoxo group and the two cobalt atoms are equivalent (Sykes and Weil 1970; Lever and Gray 1978).

Electron transfer reactions of the superoxo complexes with a variety of one-electron reductants have been reported earlier and in all those reactions the redox reactions are known to occur at the dioxygen bridge and not at the cobalt centre (Sykes and Weil 1970; Sykes 1974; Lever and Gray 1975). Recently, electron transfer reactions of superoxo complexes with strong reducing agents such as excited $Ru(bpy)_3^{2+}$ and $Ru(phen)_3^{2+}$ ions (Chandrasekaran and Natarajan 1980, 1981), unstable metal ions (Natarajan and Raghavan 1980a), organic radicals (Natarajan and Raghavan 1981) and free superoxide ion (Natarajan and Raghavan 1980b) have been reported and in all those reactions the products are the corresponding peroxo complexes. Redox process of these dioxygen complexes with Fe^{2+}, $Co(bpy)_3^{2+}$, $Co(phen)_3^{2+}$, $Fe(phen)_3^{2+}$ and the peroxo complex, $[(en)_2Co(\mu\text{-}O_2, NH_2)Co(en)_2]^{3+}$ occur by an outer-sphere electron transfer mechanism (Sykes 1974; Chandrasekaran and Natarajan 1980). Recently, attempts have been made to calculate the self exchange rate constants for the superoxo/peroxo couples using the Marcus relationship (Michelson *et al* 1977; McLendon and Mooney 1980; Chandrasekaran and Natarajan 1981). In order to calculate the above self exchange rate constants, a systematic study of the thermodynamics of interconversion of μ-superoxo and μ-peroxo complexes in terms of fairly accurate reduction potentials, (E values vs. normal hydrogen electrode) is required. Vleck (1960) and Hanslik and Vleck (1973) reported polarographic reduction of μ-superoxo complexes while Martell and co-workers (Harris *et al* 1980) employed cyclic voltammetry to determine the peak potentials for the oxidation of the peroxo complexes to the corresponding superoxo complexes. The observed redox potentials are interpreted in terms of metal-dioxygen bonding and the concept of charge-transfer from cobalt(II) to the dioxygen ligand. McLendon and Mooney (1980) and later Richens and Sykes (1982) have studied the electrodic reduction of some of the superoxo complexes using Pt electrodes in aqueous media. In the present investigation detailed cyclic voltammetric studies have been carried out for both the superoxo and the peroxo complexes by changing the ionic strength and pH of the solution. Cyclic voltammetry provides redox potentials as well as more information about the mechanistic details of electrode reactions of these complexes.

2. Experimental

Cyclic voltammetric studies were carried out for the following μ-superoxo and μ-peroxo complexes.

1. $[(NH_3)_5Co(\mu\text{-}O_2)Co(NH_3)_5](NO_3)_5$
2. $[(NH_3)_4Co(\mu\text{-}O_2, NH_2)Co(NH_3)_4](NO_3)_4$
3. $[(en)_2Co(\mu\text{-}O_2, NH_2)Co(en)_2](NO_3)_4$
4. $[(phen)_2Co(\mu\text{-}O_2, NH_2)Co(phen)_2](ClO_4)_4 \cdot 2H_2O$
5. $[(bpy)_2Co(\mu\text{-}O_2, NH_2)Co(bpy)_2](ClO_4)_4 \cdot H_2O$
6. $[(en)_2Co(\mu\text{-}O_2, NH_2)Co(en)_2](NO_3)_3$

7. $[(phen)_2Co(\mu\text{-}O_2, NH_2)Co(phen)_2](ClO_4)_3 \cdot H_2O$
8. $[(bpy)_2Co(\mu\text{-}O_2, NH_2)Co(bpy)_2](ClO_4)_3 \cdot 2H_2O$

The superoxo complexes 1–3 were prepared using the literature method (Davies *et al* 1972). Complexes 4–8 were prepared using the methods already reported with modifications (Mori and Weil 1967, 1968; Sasaki and Fujita 1969, 1970; Davies and Sykes 1971; Gileadi *et al* 1975). The dioxygen complexes were characterized by UV and visible spectra after recrystalization. A Hitachi Model 320 UV-visible spectrophotometer was used for spectral measurements. Cyclic voltammograms were run using PAR model 173 potentiostat/galvanostat. A PAR model 175 universal programmer was used to generate the cyclic triangular wave. Current output was monitored using PAR model 176 current follower. A Perkin–Elmer Hitachi 057 *X-Y* recorder was used for recording the cyclic voltammograms. The electrochemical cell was a three-electrode cell, cylindrical in shape with two sockets in which were inserted the working electrode and the counter electrode. The working electrode and the counter electrodes were platinum foils of one cm^2 area. A saturated calomel electrode placed in the side arm was the reference electrode and was connected to the potentiostat through a electrometer probe. Electrolytic contact was made by a luggin capillary projecting towards the working electrode. The platinum electrodes were cleaned and electrochemically treated prior to running a cyclic voltammogram. The condition of the working electrode was ascertained by running a cyclic voltammogram in 0·5 M H_2SO_4 in the range +1·3 and −0·2 V vs. SCE at a potential scan rate of 50 mV/sec and compared with that reported in the literature (Sawyer and Roberts 1974; Gileadi *et al* 1975). The reagents hydrochloric acid, nitric acid, sulphuric acid, sodium nitrate, sodium sulphate and sodium perchlorate were AnalaR grade supplied by BDH or E Merck.

Cyclic voltammograms were run in aqueous media at 25°C. The solutions for the cyclic voltammetric experiments contained usually 1×10^{-3} M of the dioxygen-bridged dicobalt(III) complex in 1×10^{-3} M acid and 0·1 M supporting electrolyte. The acids used were perchloric acid, sulphuric acid, nitric acid and hydrochloric acid, and the supporting electrolytes were sodium perchlorate, sodium sulphate, sodium nitrate and potassium chloride, respectively. Solutions were deoxygenated by passing a stream of oxygen-free N_2 gas through the solution kept in the cell for 30 minutes prior to the potential sweep. Potential sweeps were carried out in the cathodic direction for superoxo complexes and in the anodic direction for peroxo complexes at scan rates (ν) 5 to 200 mV/sec. Experiments were carried out by varying the acidity and ionic strength for all the dioxygen complexes. Measured reduction potentials (E_{ob}) were the mean values of the anodic (E_{pa}) and cathodic (E_{pc}) peak potentials at a given scan rate. The potential values mentioned hereafter are with reference to the normal hydrogen electrode (NHE) at 25°C.

3. Results

μ-Superoxo complexes are stable in solution with pH < 3 while the μ-peroxo complexes are stable in neutral or alkaline solution. In the case of μ-peroxo complexes 7 and 8 the complexes are stable even at pH = 1 without appreciable protonation of the peroxo group. Protonation is said to be absent in μ-superoxo

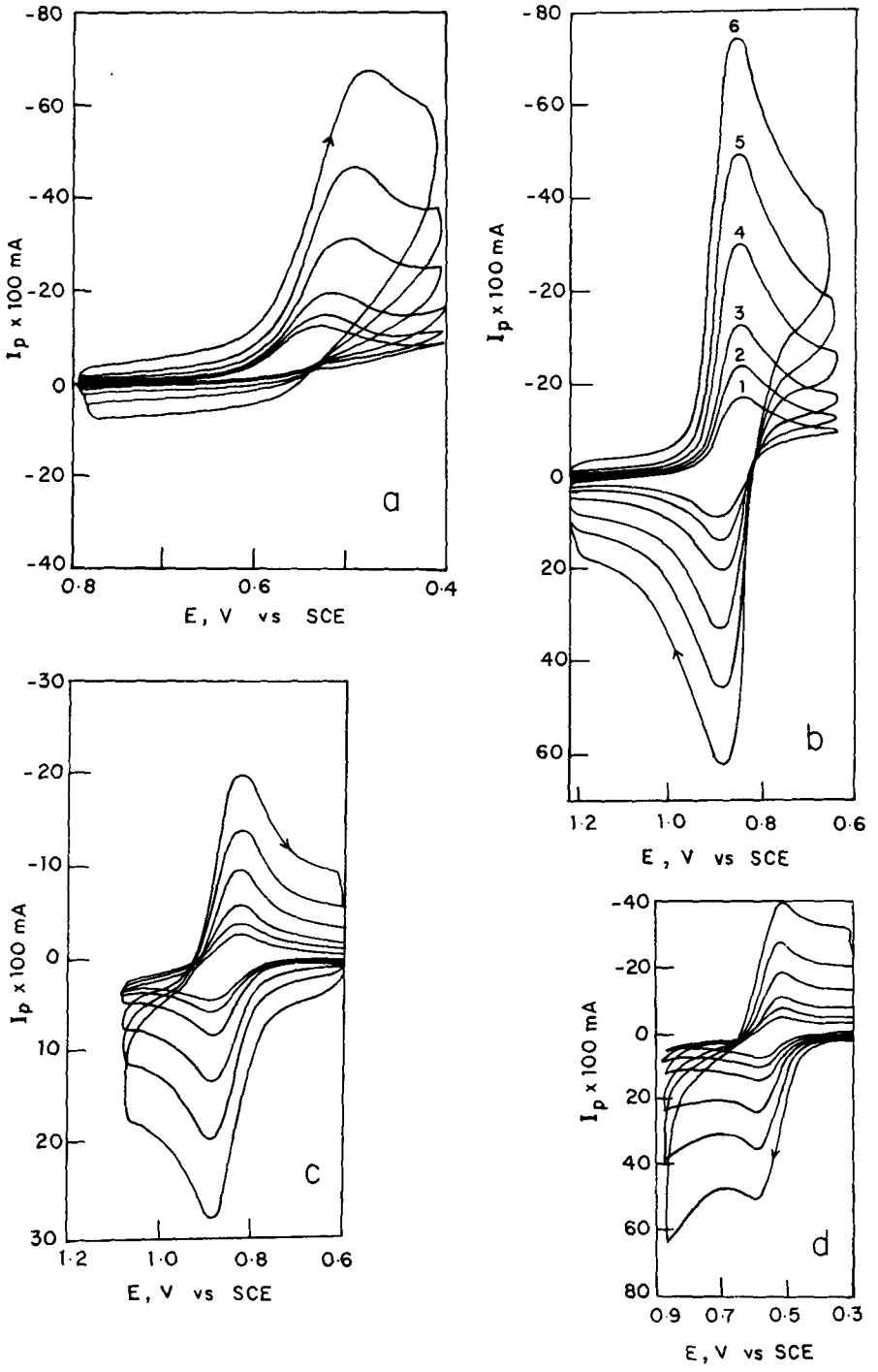

Figure 1. a,b,c,d.

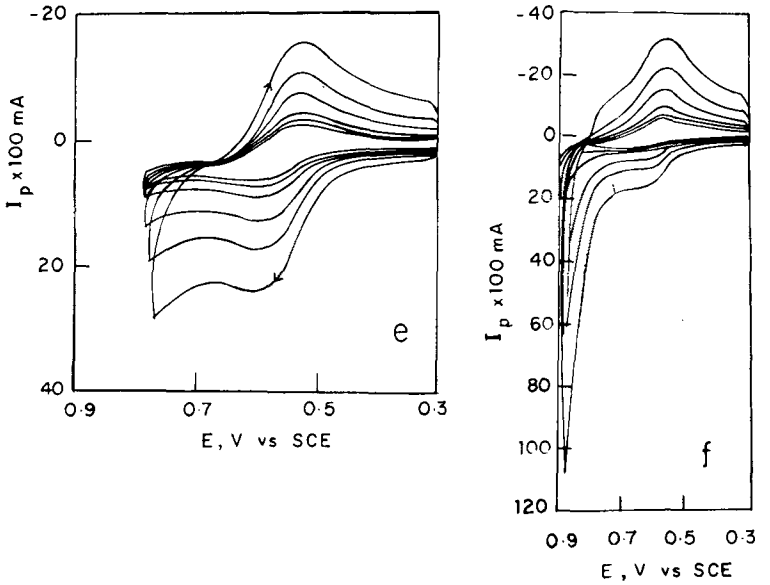

Figure 1. Cyclic voltammograms of dioxygen-bridged dicobalt(III) complexes at scan rates 5, 10, 20, 50, 100 and 200 mV/sec. (**a**) $[(NH_3)_5Co(\mu\text{-}O_2)Co(NH_3)_5](NO_3)_5$ in 0·05 M $HClO_4$; [complex] = $1{\cdot}185\times10^{-3}$ M; [$NaClO_4$] = 0·1 M. (**b**) $[(bpy)_2Co(\mu\text{-}O_2, NH_2)Co(bpy)_2](ClO_4)_4\cdot H_2O$ in 0·2 M HNO_3; [complex] = $2{\cdot}009\times10^{-3}$ M; [KNO_3] = 0·1 M. (**c**) $[(bpy)_2Co(\mu\text{-}O_2, NH_2)Co(bpy)_2](ClO_4)_3\cdot 2H_2O$ in 0·01 M H_2SO_4; [complex] = 5×10^{-4} M; [Na_2SO_4] = 0·1 M. (**d**) $[(en)_2Co(\mu\text{-}O_2, NH_2)Co(en)_2](NO_3)_3$ in 1×10^{-3} M $HClO_4$; [complex] = $1{\cdot}007\times10^{-3}$ M; [$NaClO_4$] = 0·1 M. (**e**) $[(en)_2Co(\mu\text{-}O_2, NH_2)Co(en)_2](NO_3)_3$ in 0·1 M $HClO_4$; [complex] = $9{\cdot}3\times10^{-4}$ M; [$NaClO_4$] = 0·1 M. (**f**) $[(en)_2Co(\mu\text{-}O_2, NH_2)Co(en)_2](NO_3)_3$ in 1·0 M $HClO_4$; [complex] = $9{\cdot}83\times10^{-4}$ M; [$NaClO_4$] = 0·1 M.

complexes (Sykes and Weil 1970; Lever and Gray 1978). The μ-peroxo complex 6 in acidic solutions undergoes isomerization reaction after fast protonation and this protonation equilibrium has been studied in considerable detail (Sykes and Weil 1970; Lever and Gray 1978). There is no observable decomposition of the dioxygen complexes during the course of the study in the media in which cyclic voltammetric experiments were carried out as is determined from the UV and visible absorption spectra. Typical cyclic voltammograms of the dioxygen complexes are given in figure 1. The values of peak potentials (E_p), peak currents (I_p) and separation in peak potentials (E_p) were measured in all cases from the cyclic voltammograms recorded at different potential sweep rates (Nicholson and Shain 1964; Sawyer and Roberts 1974) (table 1). For a reversible electrode couple, the peak current is related to the potential scan rate and the concentration of the complex by the expression (Nicholson and Shain 1964; Sawyer and Roberts 1974; Gileadi *et al* 1975),

$$|I_p| = 2{\cdot}72\times10^5 n^{3/2} D^{1/2} C_0 \nu^{1/2},$$

where I_p = peak current in amperes; D = diffusion coefficient in cm^2/sec; n = number of electrons involved in the electrode process, C_0 = concentration of the complex in moles/litre and ν = potential scan rate in volts/sec. Plots of I_{pc} or I_{pa}

Table 1a. Peak potentials and peak currents at different scan rates for the complex $[(NH_3)_5Co(\mu\text{-}O_2)Co(NH_3)_5](NO_3)_5$.

ν(mV/sec)	E_p(V) vs. NHE	$I_p(\mu$ A)	$I_p/\nu^{1/2}$
5	0·788	95	42·5
10	0·778	130	41·1
20	0·768	180	40·3
50	0·758	280	39·6
100	0·747	410	41·0
200	0·735	560	39·6

$[HClO_4] = 0{\cdot}05$ M; $[NaClO_4] = 0{\cdot}1$ M; [Complex] $= 1{\cdot}185 \times 10^{-3}$ M; sweep range = +0·8 to +0·4 V.

Table 1b. Peak potentials, peak currents and difference in peak potentials at different scan rates for the complex $[(phen)_2Co(\mu\text{-}O_2, NH_2)Co(phen)_2](ClO_{44})_4 \cdot H_2O$.

ν(mV/sec)	E_p(V) vs. NHE	ΔE_p(mV)	$I_{pa}(\mu$ A)	$I_{pc}(\mu$ A)	$I_{pa}/\nu^{1/2}$	$I_{pc}/\nu^{1/2}$	I_{pa}/I_{pc}
5	1·073	55	70	70	31·25	31·25	1·00
10	1·073	55	100	100	31·65	31·65	1·00
20	1·073	55	130	130	29·08	29·08	1·00
50	1·073	55	205	220	29·00	31·12	0·95
100	1·073	55	290	320	29·00	32·00	0·91
200	1·073	55	370	430	26·17	30·41	0·86

$[H_2SO_4] = 0{\cdot}1$ M; $[Na_2SO_4] = 0{\cdot}1$ M; [complex] $= 1{\cdot}014 \times 10^{-3}$ M; sweep rate = +1·2 to +0·6 V.

vs. $\nu^{1/2}$ are linear for complexes 2 to 8 in weakly acidic solutions (figure 2) and from the slopes of the above plots, the values of the diffusion coefficients were calculated. The values of peak potentials (E_p), separation of peak potentials (ΔE_p) and the values of diffusion coefficient (D) are tabulated (tables 2a–e) for complexes 2 to 8 at different acidities and ionic strengths of the medium. Redox potentials of the superoxo-bridged complexes at pH = 1 or 3 determined in the present investigation are shown in table 3.

4. Discussion

The peroxo ion having two electrons in the π_{2p} antibonding level is the least stable among the dioxygen species. In aprotic media, the peroxide dianion is a highly unstable species. When protons or metal ions stabilize the peroxide dianion the redox potentials are known to be altered (Sawyer and Valentine 1981). When the peroxide ion is coordinated to a metal ion, the stability increases as there is withdrawal of electronic charge from the peroxo group. Conversion of a superoxo to a peroxo complex is a thermodynamically favourable reaction.

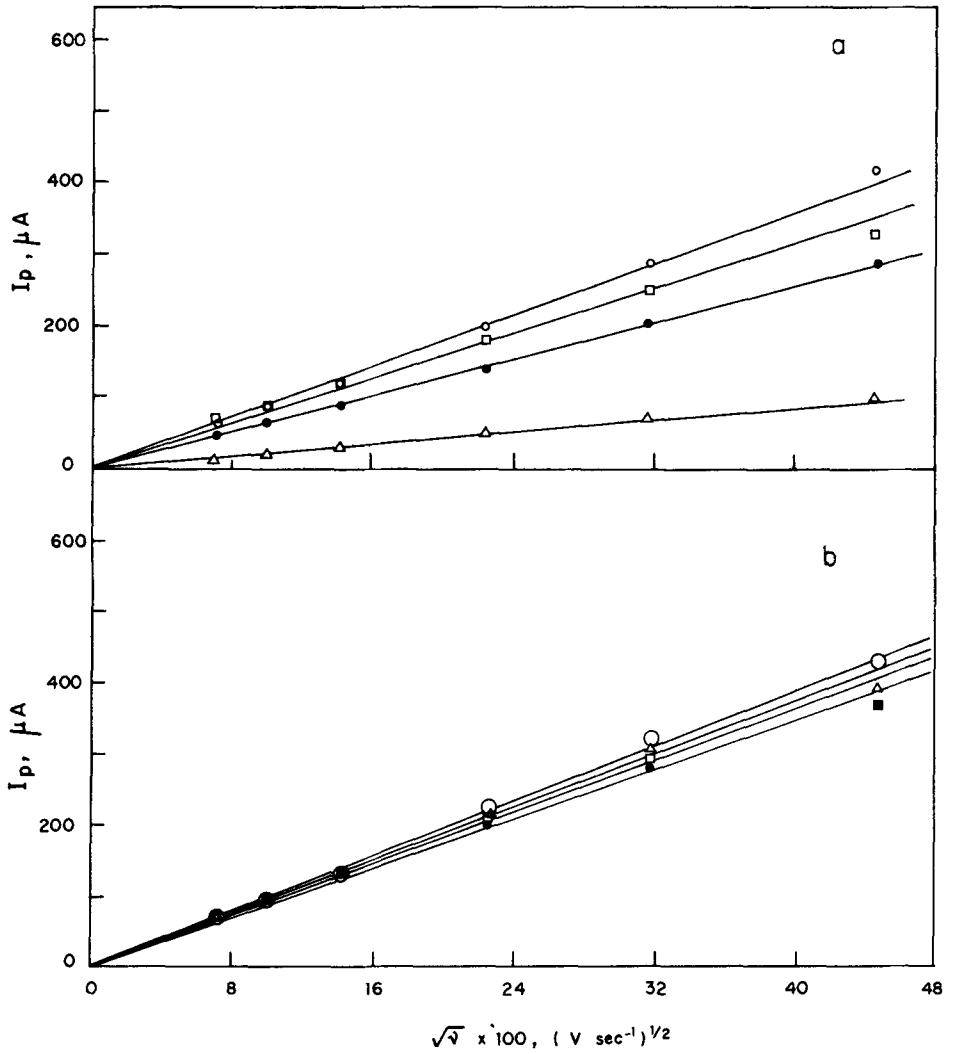

Figure 2a. I_p vs. $\nu^{1/2}$ plots for the complex $[(en)_2Co(\mu\text{-}O_2, NH_2)Co(en)_2](NO_3)_3$. (i) [complex] = $1{\cdot}007\times10^{-3}$ M; $[HClO_4] = 1\times10^{-3}$ M; $[NaClO_4] = 0{\cdot}1$ M; $\circ - I_{pa}$ vs. $\nu^{1/2}$; $\square - I_{pc}$ vs. $\nu^{1/2}$. (ii) [complex] = $0{\cdot}983\times10^{-3}$ M; $[HClO_4] = 1{\cdot}0$ M; $[NaClO_4] = 0{\cdot}1$ M; $\triangle - I_{pa}$ vs. $\nu^{1/2}$. (iii) [complex] = $0{\cdot}930\times10^{-3}$ M in 75% CH_3CN; [NaCl] = 0·1 M; $\bullet - I_{pa}$ vs. $\nu^{1/2}$. (**b**) (i) $[(phen)_2Co(\mu\text{-}O_2, NH_2)Co(phen)_2](ClO_4)_4$; [complex] = $1{\cdot}005\times10^{-3}$ M; $[H_2SO_4] = 0{\cdot}1$ M; $[Na_2SO_4] = 0{\cdot}1$ M; $\circ - I_{pc}$ vs. $\nu^{1/2}$; $\square - I_{pa}$ - vs. $\nu^{1/2}$. (ii) $[(phen)_2Co(\mu\text{-}O_2, NH_2)Co(phen)_2](ClO_4)_3$; [complex] = $1{\cdot}002\times10^{-3}$ M; $[HNO_3] = 0{\cdot}1$ M; $[KNO_3] = 0{\cdot}1$ M; $\triangle - I_{pa}$ vs. $\nu^{1/2}$; $\bullet - I_{pc}$ vs. $\nu^{1/2}$.

The superoxo complexes 2 to 5 and the peroxo complexes 6, 7 and 8 show reversible one-electron transfer process at the electrode. The apparent deviation from the reversibility of the superoxo complexes 2, 3 and 6 at higher acidity is explained on the basis of the protonation of the peroxo species in homogeneous solution. The absence of anodic peak for the ammine complex 1 in 0·05 M $HClO_4$ can be attributed either to the slow heterogeneous electron transfer of the reduced

Table 2a. Peak potentials, difference in peak potentials and diffusion coefficients for the complex $[(en)_2Co(\mu\text{-}O_2, NH_2)Co(en)_2](NO_3)_4$ at different $[H^+]$ and ionic strength.

[Medium](M)				
H^+	Supporting electrolyte	E_p(V) vs. NHE	ΔE_p(mV)	$D\times10^5$ (cm^2/sec)
$HClO_4$	$NaClO_4$			
0·0005	0·1	0·770	63	1·868
0·0010	0·1	0·773	63	1·668
0·0050	0·1	0·768	66	1·512
0·0100	0·1	0·773	71	2·164
0·5000	0·1	0·810	73	2·138
0·0010	0·05	0·778	65	1·515
0·0010	0·20	0·766	62	1·515
0·0010	0·40	0·763	65	1·415
H_2SO_4	Na_2SO_4			
0·0005	0·1	0·708	60	1·719
0·0010	0·1	0·713	62	1·714
0·0025	0·1	0·708	70	1·647
0·0010	0·05	0·703	65	1·450
0·0010	0·4	0·683	65	1·258

$\nu = 50$ mV/sec; [complex] $= 1\times10^{-3}$ M; sweep range $= +0{\cdot}8$ to $+0{\cdot}35$ V.

Table 2b. Peak potentials, difference in peak potentials and diffusion coefficients for the complex $[(en)_2Co(\mu\text{-}O_2, NH_2)Co(en)_2](NO_3)_3$ at different $[H^+]$.

$[HClO_4]$(M)	E_p(V) vs. NHE	ΔE_p(mV)	$D\times10^6$ (cm^2/sec)
0·001	0·774	70	10·030
0·100	0·778	60	2·238
1·000	0·818	56	0·715
*75% CH_3CN	0·773	60	6·053

$\nu = 50$ mV/sec; [complex] $= 1\times10^{-3}$ M; sweep range $= +0{\cdot}3$ V to $+0{\cdot}9$ V;
* [complex] $= 9{\cdot}30\times10^{-4}$ M; supporting electrolyte $= 0{\cdot}1$ M NaCl.

Table 2c. Peak potentials, difference in peak potentials and diffusion coefficients for the complex $[(phen)_2Co(\mu\text{-}O_2, NH_2)Co(phen)_2](ClO_4)_3 \cdot H_2O$ at different $[H^+]$ and ionic strength.

[Medium] (M)				
H^+	Supporting electrolyte	E_p(V) vs. NHE	ΔE_p(mV)	$D \times 10^5$ (cm^2/sec)
HNO_3	KNO_3			
0·001	0·1	1·088	59	1·420
0·010	0·1	1·086	58	1·278
0·110	0·1	1·075	60	1·147
0·210	—	1·060	60	1·188
0·410	—	1·040	59	1·226
1·100	—	1·010	65	1·352
H_2SO_4	Na_2SO_4			
0·001	0·1	1·088	57	1·242
0·020	0·1	1·083	57	1·117
0·120	0·1	1·053	57	1·147
0·010	—	1·108	60	1·114
0·020	—	1·088	60	1·117
0·110	—	1·063	59	1·077
0·210	—	1·058	55	1·147
0·410	—	1·043	58	1·077
1·000	—	1·008	62	0·959

$\nu = 50$ mV/sec; [complex] $= 5 \times 10^{-4}$ M; sweep range = 0·6 to 1·1 V.

Table 2d. Peak potentials, difference in peak potentials and diffusion coefficients for the complex $[(bpy)_2Co(\mu\text{-}O_2, NH_2)Co(bpy)_2](ClO_4)$. H_2O at different $[H^+]$ and ionic strength.

[Medium] (M)				
H^+	Supporting electrolyte	E_p(V) vs. NHE	ΔE_p(mV)	$D \times 10^5$ (cm^2/sec)
HNO_3	KNO_3			
0·1	0·1	1·036	62	1·511
0·2	0·1	1·050	64	1·549
0·3	0·1	1·043	62	1·563
0·4	0·1	1·036	65	1·541
1·0	0·1	1·033	62	1·518
H_2SO_4	Na_2SO_4			
0·050	0·1	1·078	55	1·376
0·100	0·1	1·068	55	1·277
0·200	0·1	1·058	60	1·352
0·300	0·1	1·048	60	1·300
0·400	0·1	1·028	60	1·222
1·000	0·1	1·003	60	1·145
0·1	—	1·076	58	1·274
0·1	0·02	1·076	58	1·196
0·1	0·50	1·068	55	1·088
0·1	1·00	1·040	58	0·927

$\nu = 50$ mV/sec; [complex] $= 1 \times 10^{-3}$ M; sweep range = +1·2 to 0·6 V.

Table 2e. Peak potentials, difference in peak potentials and diffusion coefficients for the complex $[(bpy)_2Co(\mu\text{-}O_2,NH_2)Co(bpy)_2](ClO_4)_3{\cdot}2H_2O$ at different $[H^+]$ and ionic strength.

[Medium](M)				
H^+	Supporting electrolyte	E_p(V) vs. NHE	ΔE_p(mV)	$D\times10^5$ (cm^2/sec)
HNO_3	KNO_3			
0·001	0·1	1·083	55	1·183
0·010	0·1	1·078	62	1·374
0·200	0·1	1·060	60	1·398
0·400	—	1·033	62	1·219
H_2SO_4	Na_2SO_4			
0·001	0·1	1·081	58	1·293
0·010	0·1	1·078	56	1·227
0·010	—	1·123	55	1·188
0·100	—	1·081	58	1·117
0·200	—	1·061	60	1·250
0·400	—	1·045	60	1·156

ν = 50 mV/sec; [complex] = 1×10^{-3} M; sweep range = +0·6 to +1·1 V

Table 3. Redox potentials of μ-superoxo bridged dinuclear cobalt(III) complexes.

Complex	pH	E(V) vs. NHE
1	1	0·760±0·005
2	3	0·763±0·005
3	3	0·800±0·010
3	3	0·725*±0·010
4	1	1·100±0·010
5	1	1·095±0·010

* In solution containing SO_4^{2-} ions.

species at the electrode or to a quasi-reversible reaction; chemical reaction followed by electrodic reduction of the superoxo complex. Decomposition of the superoxo complex 1 in aqueous acidic medium has also been reported in the reduction of the complex using Fe^{2+} as the reductant. In a similar way for complex 1 there is fast protonation of the peroxo complex formed at the electrode in the reduction process which subsequently undergoes charge transfer decomposition as follows.

$$[(NH_3)_5Co(\mu\text{-}O_2)Co(NH_3)_5]^{5+} \xrightarrow[\text{at electrode}]{+e,\ H^+} 2Co^{2+}+10NH_4^+ + O_2$$

Barnartt and Charles (1962) observed quantitative evolution of oxygen when this complex underwent reduction at platinum electrode. Unlike the above monobridged superoxo complex, the following monobridged complexes [(en)

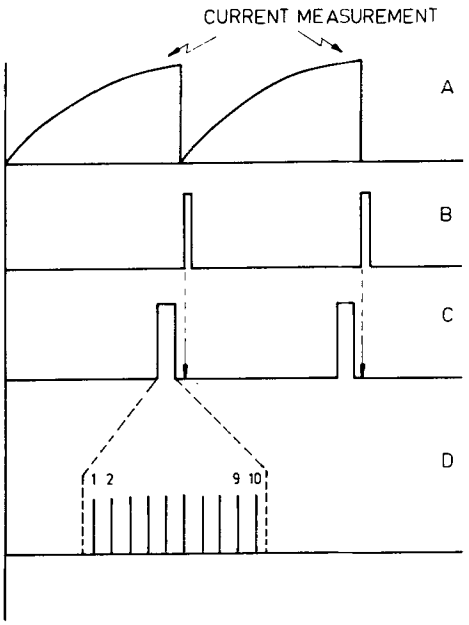

Figure 5. Timing diagram showing the relationship of various pulses to the drop time. A. Area change within a drop time, B. drop knocker pulse train, C. command pulse train generated by command pulse generator, arrow denotes drop fall, D. position of sampling pulse train in a drop life.

gate. As a result of these operations, each wave of the cell current occurring within the sampling interval gets sampled at instants corresponding to successive positive peaks of applied voltage. The time constant R_gC_g of SH is such, that it averages the sampled data. The output of SH is recorded against DC potential.

It is worthwhile to point out that circuit elements should not introduce any spurious phase change. Such phase changes would vitiate the results because the applied voltage then loses its reference character.

'*IR* compensation' is provided by positive feed back (McKubre and Macdonald 1984, p. 49). The positive feed back is obtained from the output of the current-to-voltage converter. The amount of '*IR* compensation' is adjusted by varying the fraction of the output that is fed-back.

4. Comparison between peak sampling and lock-in-amplifier (LIA) techniques

In LIA technique, the signal $[I \sin(\omega t + \varphi)]$ is multiplied by a reference square wave and the product averaged by passing through a low pass filter (LPF). It is easily shown that the in-phase component is recovered when the reference square wave is in-phase with the applied voltage. For this case the output of LIA will be

$$V_{LIA} = (2/\pi) V_x \cos \varphi, \tag{7}$$

where V_s is proportional to the amplitude I. Comparing (7) with (6) it is seen that peak sampling technique gives signals that are $(\pi/2)$ times larger than LIA.

In the case of LIA, improvement in signal-to-noise ratio (SNR) is determined by the band width of LPF, which is equal to $1/4RC$ (Hieftje 1972). Since peak sampling technique is a box-car integration (BCI) process, its noise rejection property would be the same as that of the BCI. For BCI SNR improvement depends on its observed time constant (t_{obs}) which is given by

$$t_{obs} = R_g C_g \cdot t_r / t_s, \tag{8}$$

where $R_g C_g$ is the charging time constant of the sample-hold, t_s is the width of the sampling pulse and t_r is the interval between successive sampling pulses. Noise rejection by BCI can be compared with that by LIA keeping in mind that for $R_g C_g > t_s$, smoothing by BCI is better than that by LPF having an $RC = t_{obs}$ (Abernethy 1970). In the experiments reported here, t_{obs} is 9 msec, and RC of LPF used in LIA is 20 msec which is greater than t_{obs} and hence noise rejection by LIA is better. The choice of frequency for the applied voltage and the need for keeping the measurement time interval small, limits the t_{obs} to 9 msec. One way of increasing t_{obs} (to improve noise rejection still further) is to increase $R_g C_g$. Then the averaging will be spread over several drops (Barker and Gardner 1958). It is worth pointing out that the scan rate should be kept small especially for large $R_g C_g$ to get a true record of the wave. This would increase polarographic 'run times'. There has to be a trade-off between the noise rejection and the time needed to record a polarogram. Another way of improving noise rejection is to sample the current at the negative peak as well.

5. Experimental

A Metrohm polarographic cell with a mercury pool as the counter electrode and SCE as the reference electrode was used with a Sargent capillary as DME. Analytical grade reagents were used without any further purification. Solutions were prepared from double distilled water. Deaeration was effected by bubbling purified hydrogen through the solution for 30 minutes. The '*IR* compensation' was adjusted by the ten-turn potentiometer connected to the output of current-to-voltage converter. The initial potential was kept at a value where there was no faradaic reaction. The fraction of positive feed-back was adjusted to a value slightly less than that needed to cause oscillations. The scan was initiated. After the completion of the scan, the flatness of the baseline was checked. The '*IR* compensation' was iteratively adjusted till the baseline became flat.

The polarograms for the peak sampling techniques were obtained by assembling a circuit similar to that shown in figure 4. A phase selective polarograph employing a circuit developed by us (Aithu Poojari *et al* 1973) was built and used for recording phase selective polarograms by LIA.

6. Results and discussions

AC polarograms of supporting electrolyte (0·1 M KCl) for a drop time of 0·5 sec and ΔE of 5 mV are shown in figure 6. The total cell current (curve a) is seen to vary considerably with E and is quite non-linear. The peak sampling technique

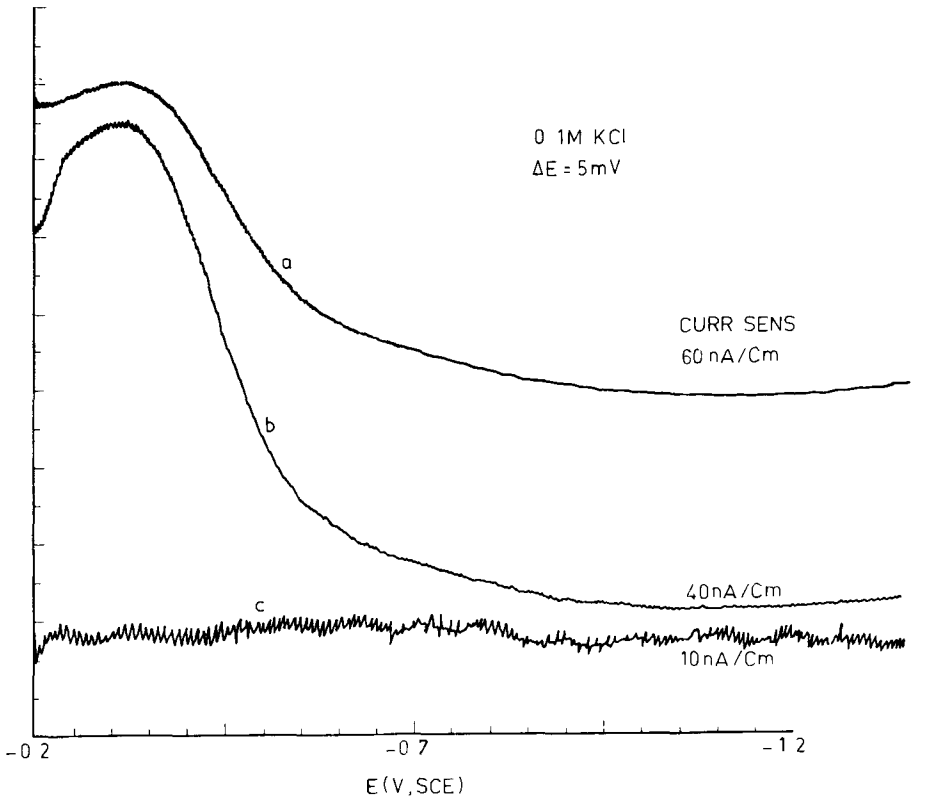

Figure 6. AC polarograms of supporting electrolyte 0·1 M KCl drop time = 0·5 sec. (a) total cell current vs. E recorded at a current sensitivity of 60 nA/cm, (b) cell current sampled at the instant when the applied voltage is a maximum; no '*IR* compensation' was used, background current is still large but less than that of curve (a), (c), 'Peak sampled' AC polarogram with '*IR* compensation'. Background current is very low and its variation with E is practically nil.

gives a polarogram (curve c) with a virtually flat baseline even at a high current sensitivity of 10 nA/cm, showing an almost perfect elimination of charging current. Curve b is obtained by using the peak sampling technique without employing *IR* compensation. Though the magnitude of charging current is less in this case as compared to curve a, it is still considerable and the baseline is quite non-linear. The difference between curve b and curve c arises from R_u. It is present in (b), while it is practically compensated in (c). The importance of *IR* compensation pointed out in §2.1 is demonstrated by the polarograms (b) and (c).

Polarograms of 5 μM each of lead, cadmium and zinc in 0·1 M KCl are shown in figure 7. The concentrations of heavy metal ions in this solution correspond to 1·0 ppm Pb^{++}, 0·6 ppm Cd^{++} and 0·3 ppm Zn^{++}. The total cell current polarogram (curve a) is seen to be similar to that due to supporting alone (curve a of figure 6). Excepting for the cadmium wave which is just visible, no other peak can be seen; thereby showing that classical AC polarography cannot be used for analysis at ppm levels. The "peak sampled" polarogram (curve c) and the "LIA phase selective" polarogram (curve d) clearly show all the three peaks. The base lines are seen to be parallel to the potential axis. Hence peak currents can be

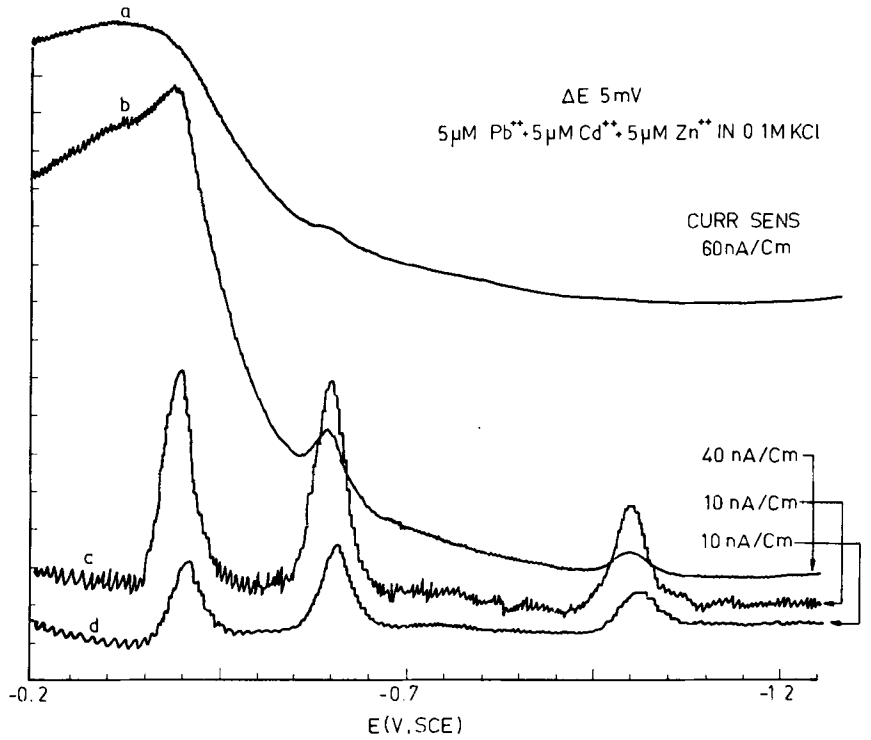

Figure 7. AC polarograms of 1·0 ppm Pb^{++} + 0·6 ppm Cd^{++} + 0·3 ppm Zn^{++} in 0·1 M KCl drop time = 0·5 sec. (a) Total cell current polarogram recorded at a current sensitivity of 60 nA/cm. Large background current has swamped completely the waves due to lead and zinc. Cadmium peak is barely visible. (b) 'Peak sampled' polarogram without '*IR* compensation' recorded at a current sensitivity of 40 nA/cm. Due to the presence of R_u, charging current elimination is incomplete. Even with a partial elimination of charging current, the cadmium and zinc peaks are seen. (c) 'Peak sampled' polarogram obtained with proper '*IR* compensation' recorded at 10 nA/cm. Peaks due to lead, cadmium and zinc are distinctly seen. (d) Phase selective polarogram using LIA technique recorded at a current sensitivity of 10 nA/cm. Proper '*IR* compensation' was used. Area of electrode in this case alone was 40% smaller. All the three peaks are distinctly seen.

measured with better accuracy. The area of the electrode used for getting 'LIA phase selective' polarograms is 40% smaller than that used for 'peak sampled' polarograms. After correcting for the difference in area, the ratios of the peak heights for the two techniques for lead, cadmium and zinc are 1·93, 1·72 and 1·93, respectively. On the basis of theory, it is shown in §4 that the wave height of a "peak sampled" polarogram should be $\pi/2$ (= 1·57) times larger than that of a "LIA phase selective" polarogram. Comparing the experimentally observed ratio with the theoretical one, it is found that the experimental values are 10 to 23% higher. Though the theoretically expected trend, viz, that peak sampling gives a larger signal as compared to LIA is verified, the quantitative agreement between theory and experiment is not very good. Further investigations are needed to understand the larger difference between theory and experiment.

As expected (§4), the noise level in peak sampled polarograms is larger than that in LIA phase selective polarogram. However, they are not unacceptably noisy. It is

possible to improve the noise level by two approaches: (a) increasing the number of samples by sampling at the negative peak, (b) averaging over a number drops as was done by Barker and Gardner (1958). These approaches have not been tried in this work.

Importance of '*IR* compensation' is demonstrated by the curve (b) which has been recorded by the peak sampling technique but without using '*IR* compensation'. Comparing curves (a) and (b) it can be inferred that there has been a partial rejection of charging current. That is the reason for the peaks due to cadmium and zinc in curve (b). At potentials anodic to $-0{\cdot}5$ V, the charging current is large and the lead wave is completely masked. The incomplete elimination of charging current in curve (b) is due to the effect of series resistance R_u. For the perfect rejection of charging current correct amount of *IR* compensation is a must.

Rapid polarography, i.e., polarography with short drop time, about 0·2 second, and large ramp rates has become popular in analytical work because polarographic "run times" are less than one minute (Bond 1970; Smith 1971). In the case of short drop times, dA/dt does not tend to a consant value even at the end of the drop life. Consequently, contribution to the charging current due to area change will exist. With a view to examine the effectiveness of peak sampling technique in eliminating charging current in 'rapid polarography', peak sampled polarograms with 0·2 sec and 1·0 sec drop times are compared in figure 8. The flatness of the base line is not

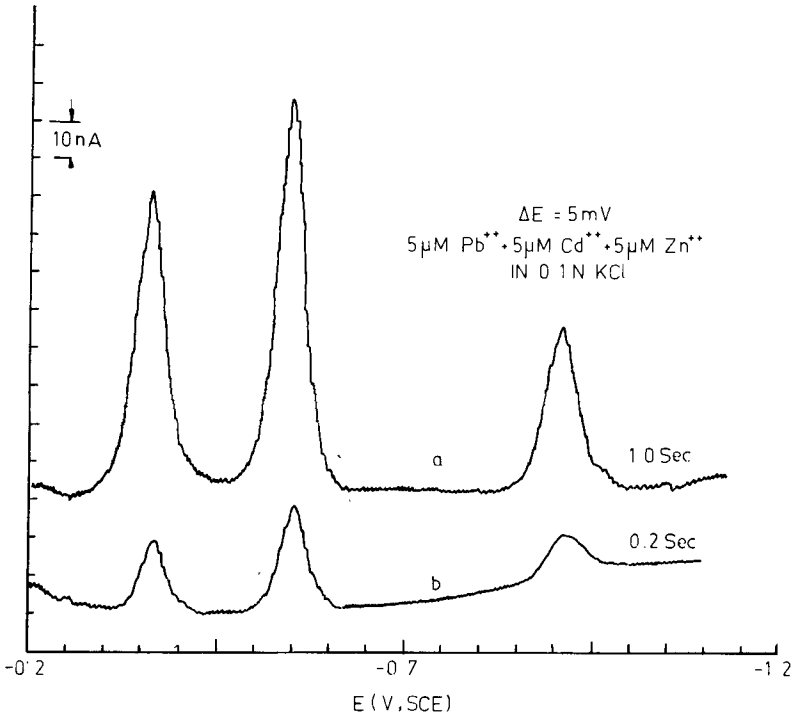

Figure 8. AC polarograms of 5 μm each of Pb^{++}, Cd^{++} and Zn^{++} in 0·1 M KCl at different drop times; (a) 'peak sampled' polarogram with drop time 1·0 sec, (b) 'peak sampled' polarogram with drop time of 0·2 sec; in both the cases all the three peaks are seen distinctly, two different DMEs were used, the ratio of the areas of DME for curves (a) and (b) is 3·7.

significantly poor in the case of the 0·2 sec drop time polarogram (curve b). The ratio of peak heights is equal to the ratio of areas of DME and hence should be the same for all the peaks. This ratio of areas is 3·7 in this work. The ratios of peak heights for lead, cadmium and zinc, respectively, are 3·6, 3·9 and 4·4. Excepting for zinc peak, the other two agree with the ratios of areas within the limits of experimental error. The larger deviation in the case of zinc is due to the incomplete elimination of charging current in the 0·2 sec drop time, whereas it is flat in the case of the polarogram with 1 sec drop time. The above results show that the peak sampling technique eliminates charging current fairly effectively in 'rapid polarography' as well.

7. Conclusions

(i) Sampling the cell current at the instant when (dE/dt) of applied voltage is zero effectively eliminates charging current in AC polarography and makes it possible to be used for analysis at sub-ppm level with good accuracy. The relative standard deviation at 0·6 ppm is 4·5%.
(ii) The signal in the peak sampling technique is larger than that of 'LIA phase selective' polarography.
(iii) The peak sampling technique eliminates charging current even in the case of 'rapid polarography'.
(iv) This technique can be considered as phase selective polarography through box-car integration.

References

Abernethy J D W 1970 *Wireless World* **Dec** p. 1
Aithu Poojary, Rajagopalan S R and Rangarajan S K 1973 *Trans. SAEST* **8** 147
Barker G C and Gardner A W 1958 AERE C/R 2297 Report, Atomic Energy Establishment, Harwell
Bond A M 1970 *Anal. Chem.* **42** 1561
Damaskin B B 1967 *The principles of current methods for the study of electrochemical reactions.* (Transl. and ed.) G Mamontov (New York: McGraw-Hill) p. 93
Hayes J W and Bauer H H 1962 *J. Electroanal. Chem.* **3** 336
Hieftje G M 1972 *Anal. Chem.* **44** 81A, (7) 69A
Malmstadt H V, Enke C G, Crouch S R and Horlick G 1974 *Optimization of electronic measurements, module 4* (California: Benjamin) p. 137
McKubre M C H and Macdonald D D 1984 *Comprehensive treatise of electrochemistry* (eds) R E White, J O M Bockris, B E Conway and E Yeager (New York; Plenum Press) vol. 8
Rehback M S and Sluyters J H 1970 *Electroanalytical chemistry* (ed.) A J Bard (New York: Marcel Dekker), vol. 4, p. 10
Smith D E 1963 *Anal. Chem.* **35** 1811
Smith D E 1966 *Electroanalytical Chemistry* **1** (ed.) A J Bard (New York: Marcel Dekker) vol. 1
Smith D E 1971 *Crit. Rev. Anal. Chem.* **2** 305
Stout D F and Kaufman M 1976 *Handbook of operational amplifier circuit design* (New York: McGraw-Hill) pp. 12–17